Research Article

Pulmonary Circulation

Optimizing imaging of the rat pulmonary microvasculature by micro-computed tomography

Yupu Deng[1], Katelynn J. Rowe[1], Ketul R. Chaudhary[1,2], Anli Yang[1], Shirley H.J. Mei[1] and Duncan J. Stewart[1,2,3]

[1]Regenerative Medicine Program, Ottawa Hospital Research Institute, Ottawa, Canada; [2]Department of Cellular and Molecular Medicine, University of Ottawa, Ottawa, Canada; [3]Division of Cardiology, Department of Medicine, University of Ottawa, Ottawa, Canada

Abstract

Micro-computed tomography (micro-CT) is used in pre-clinical research to generate high-resolution three-dimensional (3D) images of organs and tissues. When combined with intravascular contrast agents, micro-CT can provide 3D visualization and quantification of vascular networks in many different organs. However, the lungs present a particular challenge for contrast perfusion due to the complexity and fragile nature of the lung microcirculation. The protocol described here has been optimized to achieve consistent lung perfusion of the microvasculature to vessels < 20 microns in both normal and pulmonary arterial hypertension rats. High-resolution 3D micro-CT imaging can be used to better visualize changes in 3D architecture of the lung microcirculation in pulmonary vascular disease and to assess the impact of therapeutic strategies on microvascular structure in animal models of pulmonary arterial hypertension.

Keywords

method, pulmonary arterial hypertension, micro-CT, vasculature, perfusion

Date received: 20 May 2019; accepted: 24 September 2019

Pulmonary Circulation 2019; 9(4) 1–9
DOI: 10.1177/2045894019883613

Introduction

Over the past 30 years, micro-computed tomography (micro-CT) has become a standard tool for evaluating disease progression and structure–function relationships in pre-clinical models.[1–3] This imaging modality produces three-dimensional (3D) images derived from hundreds of two-dimensional (2D) projections taken from many angles around a target specimen.[1,2] The high-resolution images generated are superior to that of ultrasound and magnetic resonance imaging. Micro-CT is used extensively in pre-clinical studies for imaging of bone,[1,2] renal,[4,5] and hepatic structure;[2] as well as in defining microvascular architecture in the heart and brain,[6,7] and in the assessment of angiogenesis.[8] It has also proved invaluable in studying diseases of the lung, including pulmonary fibrosis and vascular leak during sepsis.[2,9]

Contrast-enhanced micro-CT has advantages over more traditional techniques used to evaluate pulmonary vasculature,[10–15] such as histological assessments in serial sections. Three-dimensional reconstruction of the pulmonary vasculature from micro-CT scans avoids random sampling errors and permits automated vessel measurements, quantification of total pulmonary vascular volume and visualization of the entire vascular tree.[12] Pulmonary arterial hypertension (PAH) is a rare disease characterized by remodeling and rarefaction of the pulmonary microvasculature that leads to increased pulmonary vascular resistance and right ventricular systolic pressure (RVSP).[16] While contrast-enhanced micro-CT has previously been used to image the 3D microvascular architecture in rat models of PAH,[14,15] the quality of the images can be variable and achieving reproducible imaging of the distal lung arterioles, which play a central role in this disease, has been challenging.

Corresponding author:
Duncan J. Stewart, Ottawa Hospital Research Institute, 501 Smyth Road, Ottawa, Ontario K1H 8L6, Canada.
Email: djstewart@ohri.ca

Contrast-enhanced micro-CT involves instillation of an X-ray dense contrast agent into the vasculature of the lungs. Different contrast agents, such as barium sulfate-gelatin mixtures or radiopaque silicon polymers (Microfil), have been used by other groups to investigate pulmonary arteries specifically.[10,17] Barium-gelatin mixtures offer greater infusion control as gelation is temperature-based, unlike Microfil which relies on time-based curing after mixing several reagents. Numerous reports describe techniques for contrast perfusion in rodent organs such as the kidneys,[4,5] heart,[6] or brain;[7] however, an optimized and reproducible method has yet to be reported for the lung microvasculature. We now describe a protocol that ensures reproducible imaging of the lung arterial microvasculature by optimizing filling of the distal lung arteriolar bed.

Methods

Animals

All experimental procedures were approved by the institutional Animal Care Committee and performed in accordance with institutional and Canadian Council on Animal Care guidelines. Adult male Sprague-Dawley (SD) rats (Charles River, Saint Constant, QC, Canada) weighing 180–200 g were injected intraperitoneally (i.p.) with 60 mg/kg monocrotaline (MCT) (Sigma-Aldrich, St. Louis, MO, USA) or sterile water (normal controls). Adult male RNU Nude rats (Charles River, Wilmington, MA, USA) weighing 180–200 g were injected i.p. with 70 mg/kg MCT or sterile water (normal controls). Animals were provided chow and water *ad libitum* and housed in the institutional animal care facility until they were collected 21 days after MCT/sterile water injection. Each figure annotates relevant animal numbers used.

Preparation of barium perfusate

Barium sulfate-gelatin perfusate was made by mixing 2.5 g gelatin (Sigma-Aldrich, St. Louis, MO, USA) with 17 mL ddH_2O and microwaving until gelatin was fully dissolved. Subsequently, 34 mL polibar plus barium sulfate suspension (E-Z-EM Canada Inc, Montreal, QC, Canada) was added to the warm gelatin and kept in a 46°C water bath to prevent gelation. Syringes for injecting the perfusate (3 cc, luer lock) were carefully filled to avoid bubbles, capped, and kept in the 46°C water bath until use.

Measuring in vivo RVSP

Rats were anesthetized (ketamine/xylazine, i.p.) and placed on a heating pad (37°C) in a supine position with cranial orientation to the surgeon. The right jugular vein was exposed by making a 2–3 cm incision from the right mandible to the right collar bone and blunt dissection was used until the jugular vein was visualized. A 3-0 silk suture was tied around the vessel and secured with a mosquito hemostat positioned near the nose of the rat to add tension to the vein. A second, loose ligature was placed downstream of the catheter insertion site. The jugular vein was cut down using iris scissors and a 3.5 French catheter (Transonic Scisense Inc, London, ON, Canada) was inserted into the vessel and placed in the right ventricle (RV) to measure RVSP. The probe was slowly and carefully removed from the RV via the jugular vein. For detailed graphics, please see Supplemental Figure S1. This *in vivo* RVSP was used below to individualize the perfusion pressure for each animal to ensure optimal contrast perfusion.

Flushing the lungs

A 24 G soft catheter attached to a 1 cc slip tip syringe was inserted into the exposed jugular vein to inject heparin into the circulation (~100 µL undiluted heparin, 100 I.U./200 g bodyweight). A tracheostomy was performed by dissecting skin, fat, and sternohyoid muscle away from the trachea. Subsequently, two 3-0 silk sutures were passed around the trachea and loosely tied. Iris-scissors were used to make an incision in the trachea upstream of the ligatures followed by insertion of the rat intubation tube, which was secured by tightening the ligatures. Flushing solution and tubing was prepared by filling a 60 cc luer lock syringe with 37°C heparinized saline (6 I.U./mL) and attaching a poly-ethylene tubing with T-connector (Harvard Apparatus, Saint Laurent, QC, Canada) also attached at one end to a disposable pressure transducer (Cook Regentec, Indianapolis, IN, USA) and to a catheter at the other (setup diagram in Supplemental Figure S2). Steady pressure was maintained during this process to clear any air bubbles from the tubing. The blunt 1″ 20 G catheter on the end of the T-tubing was inserted into the exposed right jugular vein, advanced into the right atrium and secured tightly with the downstream ligature. Maintaining supine position, the rat was rotated 180° to be in caudal orientation. A large, lateral incision was made across the rat's abdomen above the hips and the internal organs were removed to one side to visualize the abdominal aorta and inferior vena cava. The abdominal aorta was partially transected, while extreme care was taken to avoid damaging the vena cava, which would interfere with efficient flushing of blood out of the lungs. Intubated animals were attached to a volume-controlled ventilator (SAR-1000 Small Animal Ventilator, CWE Inc.) with a tidal volume of 10 mL/kg at 80 breaths/min for continuous ventilation throughout the rest of the procedure. Flushing via the jugular vein was accomplished by hand injection with a 60 cc syringe at a flow rate of ~20 mL/min while maintaining perfusion pressure matching the *in vivo* RVSP (monitored by pressure transducer) until the flushing solution draining from the abdominal aorta ran clear. This step typically required up to 180 mL of heparinized saline, with the syringe being detached and refilled as necessary. The operators ensured there were no air bubbles introduced

to the tubing during the process of refilling the syringe. Once the adequacy of flushing was confirmed by visualizing the whiteness of the lungs after dissecting the diaphragm, the chest was then opened via median sternotomy and the thymus and left atrial (LA) appendage were removed. For a detailed schematic, please see Supplemental Figure S3.

Barium perfusate infusion

The flushing catheter was removed from the jugular vein and replaced with a new poly-ethylene T-tube, connected at one end to a 14 G blunt catheter to insert into the main pulmonary artery (mPA), while the other end was connected to a 60 cc syringe filled with 37°C heparinized saline. The T-tube assembly was then connected to the pressure transducer via its vertical cannula (see Supplemental Figure S2 for setup diagram). Two 3-0 silk sutures were passed and loosely tied around the mPA after it was separated from the aorta. A small incision was made in the right ventricular outflow tract (RVOT), and the 14 G catheter was inserted into the mPA and secured by tightening one ligature. The inferior vena cava and descending aorta were severed, and the mPA was flushed with 37°C heparinized saline, at a pressure matching the RVSP measured *in vivo*, until the chest cavity was free of blood and the solution draining from the severed LA appendage ran clear. This step typically required 30–60 mL of heparinized saline.

Next, a 30 cc luer lock syringe filled with heparinized saline from the 46°C water bath was attached to the T-tubing and flushed through the lungs while maintaining *in vivo* RVSP as the perfusion pressure. Temperature loss during syringe attachment to the tubing and subsequent perfusion resulted in a lung temperature of 37–39°C during the infusion. The pre-filled 3 cc syringe containing barium-gelatin perfusate was removed from the 46°C water bath and then connected to the T-tubing. The pulmonary arterial circulation was perfused until the point at which no more perfusate could be injected without exceeding the *in vivo* RVSP measured prior to perfusion. Once completed, the catheter was removed from the pulmonary artery, which was closed via tightening of the second ligature. Care must be taken while removing the catheter not to spill any barium perfusate into the chest cavity. This can be controlled by applying light suction with the syringe attached to the tubing as the catheter is removed from the mPA. A detailed schematic of the barium instillation procedure is provided in Supplemental Figure S3.

Lung fixation

Following barium-gelatin perfusion, the intubation tube in the rat's trachea was detached from the ventilator and attached to a gravity-assisted formalin (10% phosphate buffered) instillation apparatus (Fig. 1a). Lungs were filled with

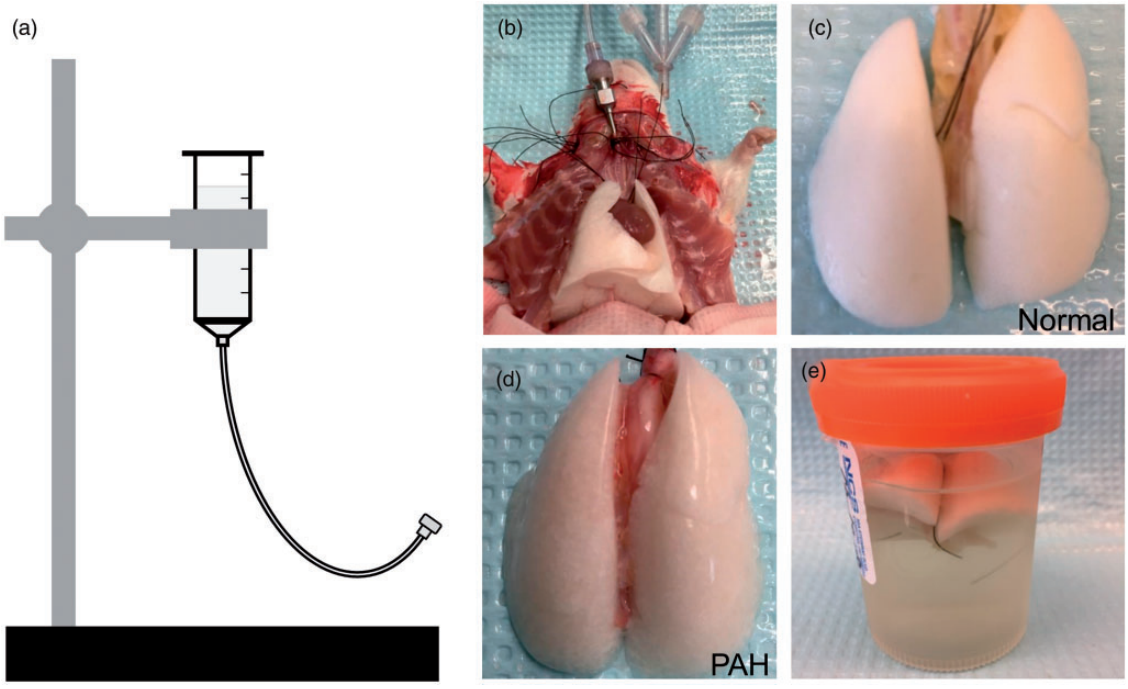

Fig. 1. Complete flushing of blood from the lungs is required for optimal contrast perfusion. (a) Gravity-assisted formalin instillation device set to fill lungs post-contrast perfusion at 15 cmH_2O. (b) After perfusing the lungs with barium, 10% phosphate buffered formalin is instilled into the lungs via the intubation tube after disconnecting from the ventilator. Well-flushed, barium-gelatin-perfused lungs are removed *en bloc* after formalin instillation (c, d). (c) Lungs from normal controls appear brilliant white following the perfusion process. (d) Lungs from PAH animals appear pinker after the perfusion process. (e) Lungs are stored in formalin at 4°C for two days before PBS rinse and long-term storage in 70% ethanol.

formalin at 15 cm H_2O until all lobes were uniformly inflated (Fig. 1b) before dissection from the chest cavity (Fig. 1c and d). The lungs and heart were removed *en bloc*. Dissected lungs were washed in 46°C water, before being transferred to 4°C formalin, to remove any external barium contamination. Lungs were stored at 4°C in formalin for two days before being rinsed 3 × 5 min in PBS and then transferred to 70% ethanol for long term storage (Fig. 1e). Samples were rinsed 3 × 5 min in PBS before scanning.

Micro-CT imaging and analysis

Samples were imaged and analyzed as previously described.[18] Briefly, the left lobes of the lungs were scanned using a desktop micro-CT (SkyScan 1272, Bruker microCT, Kontich, Belgium). Samples were imaged with the Cu 0.11 mm filter at 100 kV, 100 μA, 16.999878 μm resolution, 0.3° rotation step, 641 projections and dimensions of 1224 × 820 (1 megapixel). NRecon software was used for back projection-reconstruction (NReconServer64bit, Bruker microCT, Kontich, Belgium). Lung tissue and blood vessels were segmented and analyzed using the CTAn software (Bruker microCT, Kontich, Belgium). CTVox software was used for volume-rendering and 3D visualization (Bruker microCT, Kontich, Belgium).

Statistical analysis

Welch's unequal variances t-test was performed for between group analyses using GrapPad Prism software version 7, unless otherwise specified.

Results

As demonstrated by the white color of the lungs in Fig. 1, this protocol achieved consistent and complete clearing of blood from the microcirculation. Of note, the perfused lungs from MCT-treated animals (Fig. 1d) did not turn as uniformly white as lungs from normal rats (Fig. 1c) due to the presence of severe arterial remodeling and occlusion of pulmonary arteries.

Importance of matching perfusion pressure with in vivo pulmonary arterial pressure for both normal and PAH lungs

In Fig. 2a, the image on the left shows a micro-CT scan from a control rat lung (*in vivo* RVSP = 27 mmHg) perfused at supraphysiological pressure (80 mmHg). Filling of the pulmonary vein (white box) and barium leakage (white arrowhead) contaminating the lung's surface are apparent. In contrast, the high-quality micro-CT scan of a normal rat lung pictured on the right was obtained by matching perfusion pressure (30 mmHg) with *in vivo* RVSP (27 mmHg). This image shows neither barium leakage nor filling of the pulmonary vein. The main pulmonary artery (mPA) is

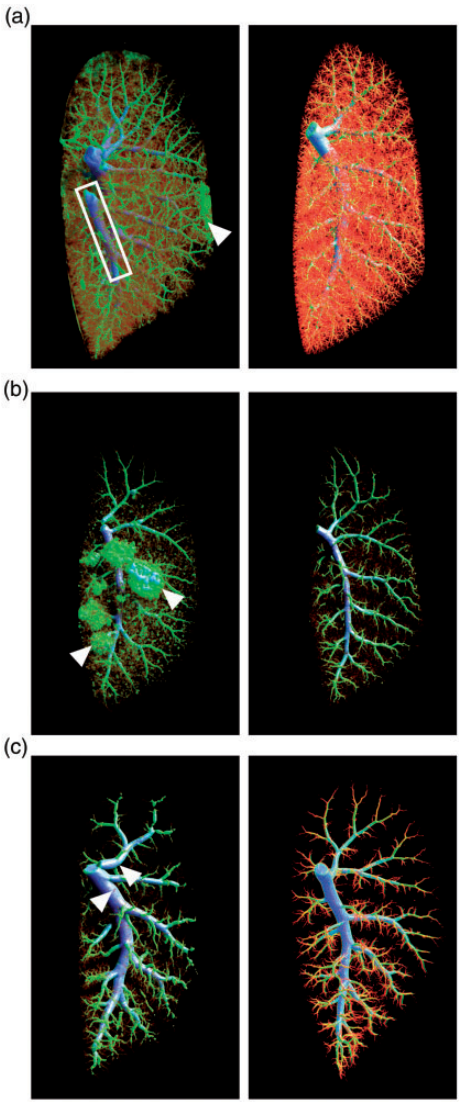

Fig. 2. Maintaining *in vivo* pressure during the perfusion process is extremely important. (a) Representative micro-CT images from normal SD rats. Left image: the left lobe (*in vivo* RVSP = 27 mmHg) perfused at 80 mmHg shows filling of the pulmonary vein (white box) and barium contamination on the outside of the lobe (white arrowhead). Right image: the left lobe (*in vivo* RVSP = 27 mmHg) shows uniform filling of the pulmonary arterial vasculature without any imperfections when perfusion pressure was maintained below 30 mmHg (n = 2). (b) Representative micro-CT images from RNU Nude rats 21 days post-MCT. Left image: the left lobe (*in vivo* RVSP = 73 mmHg) perfused at 120 mmHg demonstrates aberrant filling where the barium has broken through the capillary beds to reach the alveoli (white arrowheads). Right image: the left lobe perfused by matching pressure with the *in vivo* RVSP of 73 mmHg shows no signs of alveolar leakage (n = 2). (c) Representative micro-CT images from SD rats 21 days post-MCT. Left image: the left lobe (*in vivo* RVSP = 102 mmHg) perfused at 120 mmHg shows bulging, overfilled vessels throughout the entire vascular tree (white arrowheads). Right image: the left lobe perfused while maintaining the *in vivo* RVSP of 83 mmHg shows an appropriately filled vascular tree that could be reliably used to quantify vascular loss (n = 2).

appropriately filled in both images as it is included when quantifying total lung volume. It should be noted that for the perfusion of normal rat lung, flushing from the jugular vein should never surpass 35 mmHg and flushing from the mPA should never surpass 30 mmHg.

Immunocompromised RNU Nude rats treated with MCT develop PAH and are a useful model for testing xenogeneic cell therapies.[19,20] The image on the left in Fig. 2b demonstrates perfusion of a PAH RNU rat lung (*in vivo* RVSP = 73 mmHg) at excessive pressure (120 mmHg) that resulted in artifacts in vascular filling during contrast infusion, with disruption and leakage into what appear to be alveolar structures (white arrowheads). The right-hand image shows the superior quality that is attainable in a PAH RNU rat when perfusion pressure is matched with *in vivo* RVSP (73 mmHg).

Figure 2c compares images of MCT-induced PAH lungs from SD rats. Perfusion with pressures only moderately higher than that those measured *in vivo* (i.e. 120 mmHg perfusion pressure for *in vivo* RVSP 102 mmHg) resulted in bulging, overfilled vessels throughout the entire vascular tree (Fig. 2c, left image, white arrowheads), which confounds the accurate quantification of lung vascular volume. Maintaining perfusion pressure at the measured RVSP of 83 mmHg, produced the high-quality image pictured second in Fig. 2c.

Reproducibility of optimized perfusion for imaging microvasculature of normal lungs

Three alternative perfusion techniques were evaluated in normal SD rats for reproducibility in comparison to the optimized protocol described here. Technique I involved opening the chest cavity and immediately perfusing via direct puncture of the RV with a syringe needle (see full method in the Supplemental file). Figure 3a shows inconsistent filling of the normal vascular bed and Fig. 3b shows the lack of homogeneous vascular clearing post-perfusion when using this protocol. Technique II was modeled after a previously published protocol[14,15] that maintained a constant perfusion rate and is described in detail in the Supplemental file. As shown in Fig. 3c and d, there was again markedly inconsistent quality of perfusion with this approach. Technique III was the method initially used as the starting point prior to optimization (full description in the Supplemental file), and details of troubleshooting encountered when developing the optimized technique can be found in Supplemental Table S1. With this technique, perfusion appeared to be much more consistent; however, there was a tendency to overfill the lung vascular bed (Fig. 3e and i) as well as evidence of inhomogeneous flushing of blood (Fig. 3f). Techniques I, II, and III were performed with heparinized saline at room temperature, without maintaining rat body temperature or monitoring perfusion pressure. As well, perfusion was performed without flushing from the jugular vein and animals were not ventilated during these procedures. Images of all specimens scanned in Fig. 3 can be found in Supplemental Figure S4.

In contrast, lungs prepared according to the optimized protocol described herein yielded consistent high-quality micro-CT images and resulted in complete flushing of lungs as shown in Fig. 3g and h. The high level of reproducibility of vascular imaging with this approach was confirmed by the low variability in quantification of total vascular volume between five normal lung images perfused with our optimized technique compared to the quantification of lungs perfused using alternative techniques I, II and III (Fig. 3i). Volumetric data broken down by mid-range vessel diameter show perfusion of vessels $< 200\,\mu m$ in diameter to be the greatest source of variability between techniques (Fig. 3j), highlighting the importance of optimizing perfusion protocols for the microvasculature. Moreover, the optimized technique had a success rate, defined as full flushing of blood from the lungs and yielding a high-quality micro-CT image, of 98% for both control and PAH lungs, compared to 74% and 85% for control and PAH animals, respectively, when using alternative technique III (Supplemental Figure S4).

Reliability of quantifying the microvascular loss in a rat model of PAH

The ability to accurately quantify changes in 3D vascular architecture is important in experimental models of PAH. Figure 4 demonstrates the ability of the optimized perfusion protocol to produce high-quality micro-CT images resulting in reproducible quantification of vascular loss in a commonly used animal model of PAH.[21] Normal control SD rats demonstrated normal lung vasculature with extensive microvascular structure (Fig. 4a), while MCT treated SD rats showed marked loss of microvascular structure (Fig. 4b). Quantification of the vascular volume from the micro-CT images showed a significant loss in total left lobe vascular volume in SD rats collected for perfusion 21 days post-MCT compared to normal controls (Fig. 4c, n = 3 for each group). Please note that while statistical significance was reached, the sample size was small with only three rats for both conditions. Each rat was perfused with pressures matching the *in vivo* RVSPs denoted in Fig. 4d. The quantification of vascular volumes broken down by vessel diameter, presented in Fig. 4e and f, support the microvascular pruning observed in the micro-CT images in Fig. 4b, as the greatest difference in volumetric data is shown in vessels $< 200\,\mu m$ in diameter. The global rarefaction of microvasculature found in the left lobes of MCT-treated SD rats was observed in all five lobes of the total lung, as demonstrated by the representative videos from micro-CT scans of normal control and MCT-induced PAH rat lungs (Supplemental Figures S5 and S6, respectively).

Discussion

Micro-CT has a broad range of applications that make it a vital imaging tool in pre-clinical research. The high-resolution

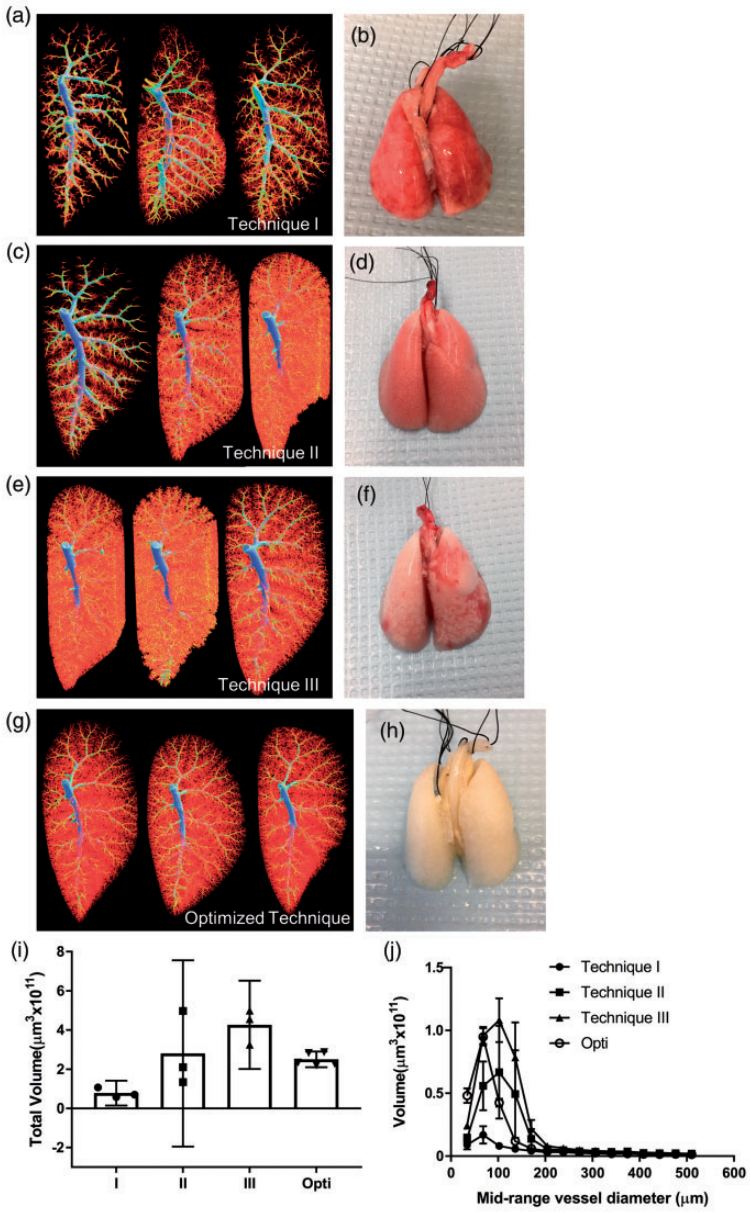

Fig. 3. Our optimized perfusion protocol successfully flushes blood from the lungs and produces more consistent micro-CT images compared to alternative perfusion techniques. (a) Micro-CT images produced by technique I (described in the Supplemental file) show sub-optimal filling, unperfused areas of vessels and pulmonary vein filling ($n = 3$). (b) Representative photo of poorly flushed lungs post-perfusion with technique I (lungs from middle micro-CT image in (a)). (c) Micro-CT images produced by technique II (described in the Supplemental file) show inconsistently filled vascular trees ($n = 3$). (d) Representative photo of poorly flushed lungs post perfusion with technique II (lungs from first micro-CT image in (c)). (e) Micro-CT images produced by technique III (described in the Supplemental file) show overfilled capillaries and unperfused regions ($n = 3$). (f) Representative photo of poorly perfused lungs that produced the middle micro-CT image in (e). (g) Uniform micro-CT images (representative) produced by our optimized perfusion technique (opti) ($n = 5$). (h) Representative photo of well-flushed lungs resulting from our optimized technique (second micro-CT image in (g)). (i) Quantification of left lobe total volume from micro-CT images shows the consistency and efficient perfusion of our optimized technique, data represent mean ± 95% CI. (j) Quantification of left lobe volume broken down by mid-range vessel diameter shows the greatest source of variability between perfusion techniques to be in vessels < 200 μm in diameter, data represent mean ± SEM.

capabilities of micro-CT imaging provide an opportunity to study detailed lung structure, in particular the organization of the complex 3D lung vascular architecture.[3] However, the complexity and fragility of the lung vasculature, especially in the context of pulmonary vascular diseases such as PAH, make it a challenging organ to reliably and reproducibly perfuse with contrast agent. To address this challenge, the present study set out to further optimize existing lung perfusion

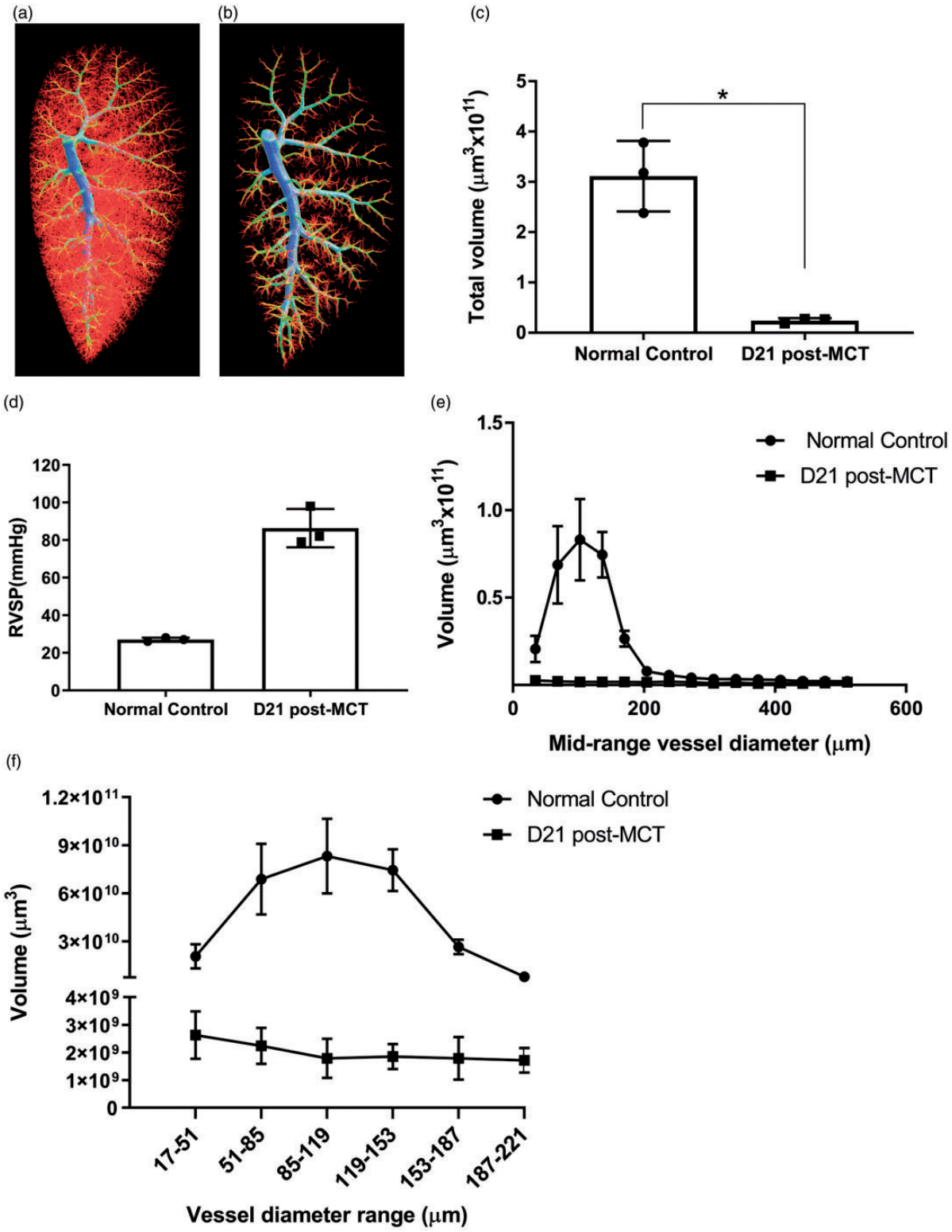

Fig. 4. SD rats with MCT-induced PAH have significantly lower total vascular volume in the left lobes of their lungs in comparison to normal age-matched controls. (a) Representative 3D vascular tree of normal SD control rat (*in vivo* RVSP = 27 mmHg). (b) Representative 3D vascular tree of PAH SD rat 21 days post-MCT injection (*in vivo* RVSP = 98 mmHg). (c) Quantification of total vascular volume in left lobes scanned with micro-CT demonstrates a significant reduction in MCT rats as determined by Welch's unequal variances t-test, *p value < 0.02. (d) *In vivo* RVSP measured in rats before perfusion that was used as a reference for the pressures maintained during the perfusion process. (e) Quantification of vascular volume broken down by mid-range vessel diameter demonstrates the greatest loss of volume in MCT-induced PAH to be in vessels $< 200\ \mu m$ in diameter. (f) Quantification of vascular volume broken down by vessel diameter range below $250\ \mu m$ highlights the difference in microvasculature between normal control and MCT-induced PAH rats, please note split y-axis. All data represent mean $\pm$ SD, n = 3 per group.

protocols for normal and PH rats. We determined that matching perfusion pressure with RVSP measured *in vivo*, maintaining physiological temperature and complete exsanguination were essential for achieving high-quality, quantifiable micro-CT images of the pulmonary vasculature.

Maintaining perfusion pressures that match the pulmonary arterial pressures measured *in vivo* was found to be the most important determinant for the quality of the micro-CT angiography. Perfusion at excessive pressures led to filling of the pulmonary vein and often caused artifacts such as distortion and aneurysmal dilatation of pulmonary arteries and extravasation of contrast agent over the lung surface or into the alveolar spaces (Fig. 2a–c), leading to inaccurate vascular volumetric analysis. Incomplete lung vascular filling with barium-gelatin perfusate in chronic hypoxia-induced PH has also been reported when perfusion pressures were too low.[17] This issue is not unique for the lung as perfusion pressure has also been reported to be a critical determinant of the adequacy of vascular imaging by micro-CT angiography for coronary,[6,22] cerebral,[7] and renal vascular beds.[4,23] However, despite the complexity of the lung microvascular 3D architecture, there has been given no previous attempt to systematically optimize lung contrast pulmonary vasculature perfusion based on *in vivo* RVSP.[14,15]

Arguably, arterial pressure is especially significant in the context of animal models of PH, as disease progression is marked by a dramatic increase in pulmonary vascular resistance and RVSP.[16] Thus, each animal has a unique pulmonary arterial pressure requiring individualization of perfusion conditions. To compare 3D vascular trees across different rats each sample needs to be consistently perfused, which requires an individualized perfusion pressure for every rat. As demonstrated by Finlay et al., different perfusion pressures were required to achieve similar quality radiographs when injecting barium-gelatin perfusate into the lungs of normal vs. chronically hypoxic (CH) rats; with CH rats requiring greater pressures for contrast infusion.[17] This may be explained by the fact that, in PAH, the microvasculature in the lung undergoes pathological structural changes that lead to arterial narrowing and loss of microcirculation by degenerative or obliterative mechanisms, resulting in higher resistance requiring greater pressures for complete filling.[7,24] In this report, the lung vasculature was perfused manually while continuously monitoring pressure using a disposable pressure transducer. Alternatively, a steady-state perfusion pump could also be used, but the settings would need to be adapted to match the *in vivo* RVSP for each individual rat.

The need for the complete removal of blood prior to contrast perfusion has previously been identified for contrast-enhanced micro-CT imaging of hind limb ischemia,[18] coronary[6,22] and cerebral vasculature,[7] and vascular leakiness in sepsis.[9] However, rigorous flushing of blood from the lungs can be challenging due to the sheer extent of the lung microcirculation and its inherent fragility. Thus, it is important to perform flushing with a closed chest cavity and maintain the rat on a ventilator to allow the heart to continue beating as long possible during the exsanguination process. Maintaining physiological temperature during flushing, by using 37°C heparinized-saline and placing the rat on a heating pad, was also found to be important for effective exsanguination (see Table S1). Vasodilators are the cornerstone for current therapy in PAH patients and are sometimes used in microvascular perfusion protocols to assist with exsanguination.[12,16,25] However, maximal dilatation of the vascular bed could lead to overestimation the pulmonary vascular volume. With the protocol described here, using heparinized-saline for all flushing steps, pre-capillary arterioles as small as 17 μm in diameter were successfully visualized without the need for vasodilators (Fig. 3j and Fig. 4e and f).

Despite its many advantages, high-resolution micro-CT does have limitations. Immense data sets are generated with each high-resolution micro-CT scan and analysis, making data storage and processing a challenge. As well, contrast-enhanced micro-CT is prone to numerous artifacts that can compromise the quality and reliability of vascular imaging. Previous publications have stressed the importance of each step in the perfusion process for consistent microvascular imaging;[3,7] for example, avoiding bubbles in the perfusion system either by using a T-tubing setup as described here or a bubble trap as described by Vasilecu et al.[25] Even small errors during the perfusion process can render samples unusable for quantification post-micro-CT imaging.

There are several specific limitations for the method presented here. While in this manuscript the micro-CT data were not validated by standard histology, it would be possible to directly compare histology vs. micro-CT within the same rat if the right main pulmonary artery was clamped to prevent influx of the perfusate into the right lobes. This would allow the contrast agent-free right lobes to be used for histology to compare directly to the micro-CT image generated from the barium-gelatin perfused left lobe. Another limitation of this study is that the alternative perfusion technique II, used to test variability, was originally performed with Microfil,[14,15] as opposed to barium-gelatin, which may partially account for the differences observed in filling of the vascular tree due to the differing properties of these contrast reagents. However, the purpose of this comparison was to highlight the importance of complete exsanguination, which is not achieved with technique II, and maintenance of *in vivo* RVSP for perfusion pressure. To maintain accurate perfusion pressures during our procedure, the initial catheter placed for flushing must be carefully positioned in the jugular vein to avoid touching the vessel wall, which would cause greater resistance and thus falsely elevated pressure readings during the perfusion. Our technique is also limited because it is a terminal procedure and therefore does not permit for longitudinal studies. While advances have been made in live micro-CT imaging of blood vessels in small animals, the rapid clearance of contrast agents and acquisition time for high resolution still limit *in vivo* micro-CT imaging of the lung vasculature.[26]

In conclusion, we have described a protocol for micro-CT contrast imaging that generates high-quality images of the microvasculature of lungs from normal control rats as well as in rats with severe PH and permits accurate and reproducible quantification of pulmonary vascular volume. This was achieved by carefully optimizing existing perfusion protocols. The high level of resolution of micro-CT imaging, along with the perfusion protocol described here, has the potential to enable studies that quantitatively evaluate novel pro-angiogenic therapies in pre-clinical models of vascular disease.

Conflict of interest

K.R.C. is a recipient of Research Fellowship from Heart and Stroke Foundation of Canada and Scholar award from Canadian Vascular Network and CIHR. D.J.S. has equity interest in Northern Therapeutics (NT) Inc., and S.M. and Y.D. have received personal fees from NT that are outside of this submitted work.

Funding

This study was partially funded by an industry-sponsored research grant (to D.J.S. and S.M.) and Canadian Institutes of Health Research Foundation Grant (to D.J.S.). The funding institution had no role in the conception, design or conduct of the study, data collection or analysis, interpretation or presentation of the data, or preparation, review or approval of the manuscript.

ORCID iD

Ketul R. Chaudhary https://orcid.org/0000-0003-1725-7438

Supplemental material

Supplemental material for this article is available online.

References

1. Boerckel JD, Mason DE, McDermott AM, et al. Microcomputed tomography: approaches and applications in bioengineering. *Stem Cell Res Ther* 2014; 5: 144.
2. Clark DP and Badea CT. Micro-CT of rodents: state-of-the-art and future perspectives. *Phys Med* 2014; 30: 619–634.
3. Zagorchev L, Oses P, Zhuang ZW, et al. Micro computed tomography for vascular exploration. *J Angiogenes Res* 2010; 2: 7.
4. Xu R, Franchi F, Miller B, et al. Polycystic kidneys have decreased vascular density: a micro-CT study. *Microcirculation* 2013; 20: 183–189.
5. Almajdub M, Magnier L, Juillard L, et al. Kidney volume quantification using contrast-enhanced in vivo X-ray micro-CT in mice. *Contrast Media Mol Imaging* 2008; 3: 120–126.
6. Toyota E, Fujimoto K, Ogasawara Y, et al. Dynamic changes in three-dimensional architecture and vascular volume of transmural coronary microvasculature between diastolic- and systolic-arrested rat hearts. *Circulation* 2002; 105: 621–626.
7. Ghanavati S, Yu LX, Lerch JP, et al. A perfusion procedure for imaging of the mouse cerebral vasculature by X-ray micro-CT. *J Neurosci Methods* 2014; 221: 70–77.
8. Ehling J, Theek B, Gremse F, et al. Micro-CT imaging of tumor angiogenesis: quantitative measures describing micromorphology and vascularization. *Am J Pathol* 2014; 184: 431–441.
9. Langheinrich AC and Ritman EL. Quantitative imaging of microvascular permeability in a rat model of lipopolysaccharide-induced sepsis: evaluation using cryostatic micro-computed tomography. *Invest Radiol* 2006; 41: 645–650.
10. Razavi H, Dusch MN, Zarafshar SY, et al. A method for quantitative characterization of growth in the 3-D structure of rat pulmonary arteries. *Microvasc Res* 2012; 83: 146–153.
11. Chandra SM, Razavi H, Kim J, et al. Disruption of the apelin-APJ system worsens hypoxia-induced pulmonary hypertension. *Arterioscler Thromb Vasc Biol* 2011; 31: 814–820.
12. Phillips MR, Moore SM, Shah M, et al. A method for evaluating the murine pulmonary vasculature using micro-computed tomography. *J Surg Res* 2017; 207: 115–122.
13. Razavi H, Stewart SE, Xu C, et al. Chronic effects of pulmonary artery stenosis on hemodynamic and structural development of the lungs. *Am J Physiol Lung Cell Mol Physiol* 2013; 304: L17–28.
14. Faight EM, Verdelis K, Zourelias L, et al. MicroCT analysis of vascular morphometry: a comparison of right lung lobes in the SUGEN/hypoxic rat model of pulmonary arterial hypertension. *Pulm Circ* 2017; 7: 522–530.
15. Shields KJ, Verdelis K, Passineau MJ, et al. Three-dimensional micro computed tomography analysis of the lung vasculature and differential adipose proteomics in the Sugen/hypoxia rat model of pulmonary arterial hypertension. *Pulm Circ* 2016; 6: 586–596.
16. Farber HW and Loscalzo J. Pulmonary arterial hypertension. *N Engl J Med* 2004; 351: 1655–1665.
17. Finlay M, Barer GR and Suggett AJ. Quantitative changes in the rat pulmonary vasculature in chronic hypoxia – relation to haemodynamic changes. *Q J Exp Physiol* 1986; 71: 151–163.
18. Schaad L, Hlushchuk R, Barré S, et al. Correlative imaging of the murine hind limb vasculature and muscle tissue by microCT and light microscopy. *Sci Rep* 2017; 7: 41842.
19. Ormiston ML, Deng Y, Stewart DJ, et al. Innate immunity in the therapeutic actions of endothelial progenitor cells in pulmonary hypertension. *Am J Respir Cell Mol Biol* 2010; 43: 546–554.
20. Suen CM, Stewart DJ, Montroy J, et al. Regenerative cell therapy for pulmonary arterial hypertension in animal models: a systematic review. *Stem Cell Res Ther* 2019; 10: 75.
21. Gomez-Arroyo JG, Farkas L, Alhussaini AA, et al. The monocrotaline model of pulmonary hypertension in perspective. *Am J Physiol Lung Cell Mol Physiol* 2012; 302: L363–L369.
22. Sangaralingham SJ, Ritman EL, McKie PM, et al. Cardiac micro-computed tomography imaging of the aging coronary vasculature. *Circ Cardiovasc Imaging* 2012; 5: 518–524.
23. Plouraboue F, Cloetens P, Fonta C, et al. X-ray high-resolution vascular network imaging. *J Microsc* 2004; 215: 139–148.
24. Chaudhary KR, Taha M, Cadete VJJ, et al. Proliferative versus degenerative paradigms in pulmonary arterial hypertension: have we put the cart before the horse? *Circ Res* 2017; 120: 1237–1239.
25. Vasilescu DM, Knudsen L, Ochs M, et al. Optimized murine lung preparation for detailed structural evaluation via micro-computed tomography. *J Appl Physiol* 2012; 112: 159–166.
26. Ashton JR, West JL and Badea CT. In vivo small animal micro-CT using nanoparticle contrast agents. *Front Pharmacol* 2015; 6: 256.